Design of a Sliding Mode-Adaptive Proportional-Integral-Derivative Control for Aerial Systems With a Suspended Load Exposed to Wind Gusts

Vincenzo Di Paola, Alexandre Goldsztejn, Matteo Zoppi, Stéphane Caro

Design of a Sliding Mode-Adaptive PID Control for Aerial Systems with a Suspended Load Exposed to Wind Gusts

Vincenzo Di Paola*
University of Genova - DIME, Genova, Italy
Nantes Université, École Centrale Nantes
CNRS, LS2N, UMR 6004
1, rue de la Noe, 44321 Nantes, France
Email: vincenzo.dipaola@edu.unige.it

Alexandre Goldsztejn
Nantes Université, École Centrale Nantes
CNRS, LS2N, UMR 6004
1, rue de la Noe, 44321 Nantes, France
Email: alexandre.goldsztejn@ls2n.fr

Matteo Zoppi
University of Genova - DIME, Genova, Italy
Email: matteo.zoppi@unige.it

Stéphane Caro
ASME Member
Nantes Université, École Centrale Nantes, CNRS
LS2N, UMR 6004, 1, rue de la Noe, 44321 Nantes, France
Email: stephane.caro@ls2n.fr

ABSTRACT

Wind gusts are among the well-known disturbances that afflict aerial systems. A tracking task for a load suspended by massless rigid bars and quadrotors is considered in this paper. The complexity of the tracking task lies in the presence of wind gusts. Therefore, a self-tuning gain techniques for a Proportional-Integral-Derivative (PID) control are introduced to accomplish tracking tasks when wind gusts appear. To automatically tune the PID gains, a sliding mode condition is exploited. The stability of this approach, considering bounded disturbances, is guaranteed by introducing a supervisory control designed through the Lyapunov method. The proposed solution and its performances were tested through simulation and compared with both PD and PID controls.

NOMENCLATURE

F_O, F_{Q_i} inertial frame, i^{th} drone frame
$\mathbf{e}_1, \mathbf{e}_2, \mathbf{e}_3$ canonical base of inertial frame (O, X, Y, Z)
$\mathbf{i}_i, \mathbf{j}_i, \mathbf{k}_i$ canonical base of drone frame (Q_i, x_i, y_i, z_i)
$m_i \in \mathbb{R}$ mass of the i^{th} drone
$m_L \in \mathbb{R}$ mass of the load
$\mathbf{x}_i, \dot{\mathbf{x}}_i, \ddot{\mathbf{x}}_i \in \mathbb{R}^3$ position, linear velocity, acceleration of the i^{th} drone in F_O

*Corresponding author.

$\mathbf{R}_i \in SO(3)$ orientation of the i^{th} robot with respect to F_O

$g \in \mathbb{R}$ gravity acceleration magnitude

$\mathbf{\Omega}_i, \dot{\mathbf{\Omega}}_i \in \mathbb{R}^3$ angular velocity, acceleration of the robot in F_{Q_i}

$f_i \in \mathbb{R}$ trust force of the i^{th} robot

$\mathbf{m}_i \in \mathbb{R}^3$ control moment of the i^{th} robot in F_{Q_i}

$\mathbf{J}_i \in \mathbb{R}^{3\times3}$ inertia tensor of the i^{th} robot in F_{Q_i}

$t_i \in \mathbb{R}$ tension magnitude along the i^{th} link

$\mathbf{q}_i \in \mathbb{S}^2$ unit vector from the drone to the load in F_O

$\boldsymbol{\omega}_i \in \mathbb{R}^3$ angular velocity of the i^{th} link in F_O

1 INTRODUCTION

Nowadays quadrotors are increasingly attracting attention from researchers due to their agility and potential ability to accomplish tasks autonomously. These peculiarities make them suitable for a wide range of applications such as filming, grasping, and collaborative transportation [1]. The deployment of a team of quadcopters enables them to overcome the payload limits that affect them as individuals. However, the use of multiple quadrotors to steer a load leads to an increase in complexities in terms of control. Within this context, among the control techniques developed so far, both geometric control [2] and flatness [3] theories recorded quite large success in the research community. Indeed, in [4], a geometric control was designed to command a team of agents transporting a point-mass load with rigid links. Furthermore, in [5], the systems (i.e. cables-quadrotors-platform) were proven to be flat. Subsequently, these works gave rise to several contributions where flatness and/or geometric control were used to perform aerial transportation tasks with a rigid platform [6, 7] and also with flexible cables [8, 9]. Recently, in [10], the geometric control [7] was implemented in a real hardware that exploited the abilities of onboard cameras to estimate the system's state and accomplish tracking tasks. As a result, this work allowed disengaging flights from Motion Capture System (MOCAP). Indeed, one of the main objectives among researchers is to empower aerial systems to be as autonomous as possible in order to let them navigate in outdoor environments autonomously. Hence, a preliminary study investigating how to cope with external disturbances by means of varying the system stiffness was conduct in [11]. With this in mind, this work tackles the issues arising from the presence of wind during aerial transportation tasks. By nature, wind includes turbulence and gusting [12]. Consequently, the wind is a stochastic and chaotic phenomenon. Thus, by analogy, the control of chaotic systems [13, 14] was inspirational for this work. In particular, a Sliding-Mode Adaptive PID (SM-APID) control that confers to a system with massless rigid links, quadrotors and a point-mass load, the ability to track a given trajectory under the effect of wind is introduced for the first time. The Dryden wind model [15] was hereby considered to test the SM-APID ability.

Therefore, one contribution of this work is related to the introduction of aerodynamic forces in the dynamical model of aerial systems with massless rigid links, quadrotors and a point mass load. Another major contribution regards the design of the SM-APID control, for the mentioned system, to address the tracking problem when gusts appear. Moreover, numerical simulations demonstrate the validity and robustness of the proposed approach with respect to the existing control methods.

The paper is organized as follows: Section 2 introduces the dynamical model of the system. Section 3 describes the control design. Section 4 presents a case study and simulation results. Finally, conclusions and future work are drawn in Section 5.

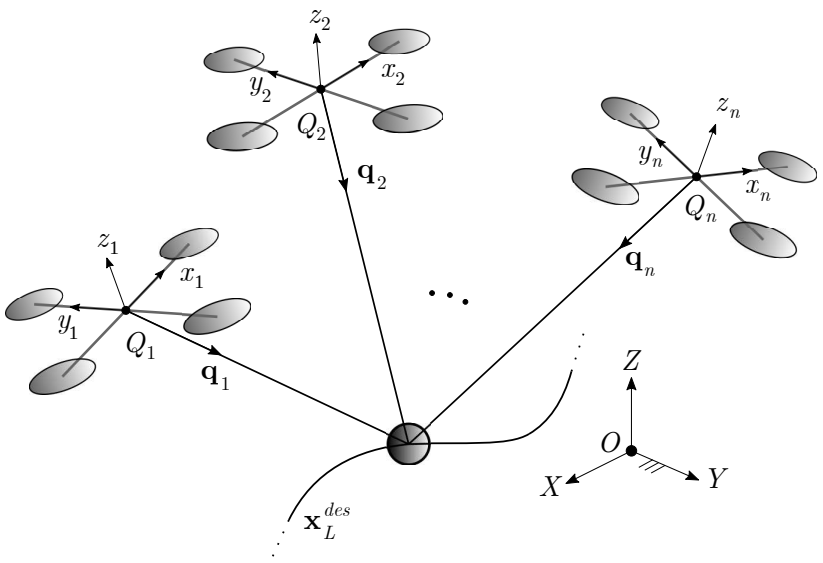

Fig. 1: Aerial System: general architecture of the aerial system considered.

2 DYNAMIC MODEL

In this work, the tracking problem was addressed by considering the system as composed of a team of n quadrotors and n massless rigid links that collaborate to carry the point-mass load along the desired trajectory as illustrated in Figure 1. The equations of motion were obtained by using the energetic method [4, 7, 16, 17]. Throughout all this paper the used symbols were summarized in the Nomenclature Section.

Since each quadrotors lies on the surface of a sphere of radius l_i i.e. length of the i^{th} link, the configuration manifold associated with the mentioned system is $\mathbb{R}^3 \times (\mathbb{S}^2 \times SO(3))^n$ where $\mathbb{S}^2 = \{\mathbf{q} \in \mathbb{R}^3 | \, ||\mathbf{q}|| = 1\}$ represents the 2-sphere set whereas $SO(3) = \{\mathbf{R} \in \mathbb{R}^{3\times3} | \, \mathbf{R}^T\mathbf{R} = \mathbf{I}, \, det(\mathbf{R}) = 1\}$ defines the Special Orthogonal Group. Recalling that the action integral for the non conservative forces is

$$\mathfrak{a} = \int_{t_0}^{t_f} (\mathcal{T} - \mathcal{U} + \mathcal{W}_f + \mathcal{W}_m) \, dt, \tag{1}$$

where $\mathcal{T}$ is the kinetic energy, $\mathcal{U}$ is the potential energy and $\mathcal{W}_f$ and $\mathcal{W}_m$ represent the works of external forces and moment, respectively. Now, Hamilton's principle of least action states that the path a conservative system takes from configurations $\mathbf{\Psi}(t_0)$ to $\mathbf{\Psi}(t_f)$, where $\mathbf{\Psi}$ is the set of generalized coordinates belonging to the configuration manifold, is the one that makes the action stationary. In mathematical terms

$$\delta\mathfrak{a} = \int_{t_0}^{t_f} (\delta\mathcal{T} - \delta\mathcal{U} + \delta\mathcal{W}_f + \delta\mathcal{W}_m) \, dt = 0, \tag{2}$$

where δ expresses the variation in the integrated quantities. Hence, integrating all these terms by parts

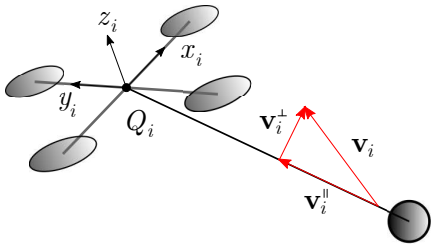

Fig. 2: Control force decomposition: representation of the i^{th} projection of the control force along a generic link.

returns the equations of motion

$$\begin{cases} \dfrac{d}{dt}\mathbf{x}_L = \dot{\mathbf{x}}_L, & (3) \\ (\sum_{i=1}^{n} m_i \mathbf{q}_i \mathbf{q}_i^T + m_L \mathbf{I})(\ddot{\mathbf{x}}_L + g\mathbf{e}_3) = \sum_{i=1}^{n} \left(\mathbf{v}_i^{\parallel} - m_i l_i ||\boldsymbol{\omega}_i||^2 \mathbf{q}_i + (\mathbf{q}_i \cdot \mathbf{f}_{i,w})\mathbf{q}_i\right) + \mathbf{f}_{L,w}, & (4) \\ \dot{\mathbf{q}}_i = \boldsymbol{\omega}_i \times \mathbf{q}_i, & (5) \\ \dot{\boldsymbol{\omega}}_i = \dfrac{1}{l_i}\hat{\mathbf{q}}_i(\ddot{\mathbf{x}}_L + g\mathbf{e}_3) - \dfrac{1}{m_i l_i}\hat{\mathbf{q}}_i \mathbf{v}_i^{\perp} - \dfrac{1}{m_i l_i}\hat{\mathbf{q}}_i \mathbf{f}_{i,w}, & (6) \\ \dot{\mathbf{R}}_i = \mathbf{R}_i \hat{\boldsymbol{\Omega}}_i, & (7) \\ \mathbf{m}_i = \mathbf{J}_i \dot{\boldsymbol{\Omega}} + \boldsymbol{\Omega}_i \times \mathbf{J}_i \boldsymbol{\Omega}_i, & (8) \end{cases}$$

where $\mathbf{f}_{i,w}$ and $\mathbf{f}_{L,w}$ are the aerodynamic forces acting on the quadrotors and the load, respectively, $\mathbf{I}$ is the identity matrix of dimension three, the vector $\mathbf{v}_i$ represents the control force of the i^{th} robot such that $\mathbf{v}_i = f_i \mathbf{R}_i \mathbf{e}_3$ whereas the vectors $\mathbf{v}_i^{\parallel}$ and $\mathbf{v}_i^{\perp}$ denote the projection of $\mathbf{v}_i$ along and normal to $\mathbf{q}_i$, respectively

$$\mathbf{v}_i^{\parallel} = (\mathbf{I} + \hat{\mathbf{q}}_i^2)\mathbf{v}_i = (\mathbf{q}_i \cdot \mathbf{v}_i)\mathbf{q}_i = \mathbf{q}_i \mathbf{q}_i^T \mathbf{v}_i, \tag{9a}$$

$$\mathbf{v}_i^{\perp} = -\hat{\mathbf{q}}_i^2 \mathbf{v}_i = -\mathbf{q}_i \times (\mathbf{q}_i \times \mathbf{v}_i) = (\mathbf{I} - \mathbf{q}_i \hat{\mathbf{q}}_i^T)\mathbf{v}_i. \tag{9b}$$

The symbol $\hat{\cdot}$ denotes the *hat map*:$\hat{\cdot} : \mathbb{R}^3 \to \mathfrak{so}(3)$ where $\mathfrak{so}(3)$ corresponds to the Lie algebra associated to the Lie group $SO(3)$. The relationship between Eqs. (9a) and (9b) is depicted in Figure 2 and it can be expressed as

$$\mathbf{v}_i = \mathbf{v}_i^{\perp} + \mathbf{v}_i^{\parallel}. \tag{10}$$

Remark 2.1. *The need to distinguish between parallel and orthogonal components comes from the structure of the equations of motion. In fact, Equation (4) governs the translational dynamics of the load and then it contains the parallel component of the control force. On the other hand, Equation (6) governs the attitude of the load and therefore includes the orthogonal component of the control force. Those properties play a central role in designing the control.*

Remark 2.2. *Compared to previous works, Equations (3)-(8) present the introduction of the wind forces acting on the quadrotors and the payload.*

3 CONTROL

The overall objective of the control is to ensure that the load follows the desired trajectory while pursuing the desired system configuration under the action of external disturbances. The *relative formation control* [4] is used. Thus, the objective is to find a set of control inputs $\mathfrak{U} = \{f_i, \mathbf{m}_i \, \forall \, i = 1, \ldots, n\}$ such that $\mathbf{x}_L \longrightarrow \mathbf{x}_L^{des}$ and $\mathbf{q}_i \longrightarrow \mathbf{q}_i^{des}$ while $t \longrightarrow \infty$.
Furthermore, to ensure insensitivity to bounded external disturbances, a SM-APID controller is designed to define a proper action that steers the load. The fusion of the two above-mentioned approaches enables to control ACTSs even in presence of external disturbances.

In the first Subsection 3.1 the structure of the SM-APID controller and aspects concerning its design are recalled. Subsection 3.2 concerns with the contribution of this work since it shows how to exploit the SM-APID control to guide the position of the load subject to external disturbances. In Subsection 3.3, the design of the orthogonal component to reach the desired configuration is done and in Subsection 3.4 the attitude control for the quadrotors is recalled for sake of completeness.

3.1 Design of the Sliding Mode-Adaptive PID control

Let us consider the description of a dynamical system in general form

$$\dddot{\tilde{\mathbf{x}}} = f(\tilde{\mathbf{x}}) + \Delta f(\tilde{\mathbf{x}}) + g(\tilde{\mathbf{x}})\mathbf{u} + \boldsymbol{\delta}, \tag{11}$$

where $\tilde{\mathbf{x}}, \dddot{\tilde{\mathbf{x}}} \in \mathbb{R}^n$ form the system' state $\mathbf{x} = [\tilde{\mathbf{x}}, \dddot{\tilde{\mathbf{x}}}]^T \in \mathbb{R}^{2n}$, $M_{\mathbf{x}}$, $f(\tilde{\mathbf{x}})$ and $\Delta f(\tilde{\mathbf{x}})$ represent the system model and the its uncertainties, $g(\tilde{\mathbf{x}})\mathbf{u}$ is the *affine* terms with $\mathbf{u}$ as control input and, the last terms $\boldsymbol{\delta}$ identifies the external disturbances. Observe that both disturbances and system uncertainties are assumed to be bounded above $\boldsymbol{\delta}(\cdot) \leq \boldsymbol{\delta}^u(\cdot)$, $f(\cdot) \leq f^u(\cdot)$ and $\Delta f(\cdot) \leq \Delta f^u(\cdot)$. A common and direct approach that can be used to define a control input consists in using the so-called *feedback linearization* techniques namely

$$\mathbf{u}^* = -g(\tilde{\mathbf{x}})^{-1}\big(f(\tilde{\mathbf{x}}) + \Delta f(\tilde{\mathbf{x}}) + \boldsymbol{\delta} + \dddot{\tilde{\mathbf{x}}}^{des} + \mathbf{k}_0\,\tilde{\mathbf{e}} + \mathbf{k}_1\dddot{\tilde{\mathbf{e}}}\big). \tag{12}$$

where $\mathbf{e} = [\tilde{\mathbf{e}}, \dddot{\tilde{\mathbf{e}}}]^T \in \mathbb{R}^{2n}$ and $\dot{\mathbf{e}} = [\dddot{\tilde{\mathbf{e}}}, \ddddot{\tilde{\mathbf{e}}}]^T \in \mathbb{R}^{2n}$ are the state error vectors which are the time derivatives of $\mathbf{e} = \mathbf{y} - \mathbf{x}$ with $\mathbf{y} = \left[\tilde{\mathbf{x}}^{des}, \dddot{\tilde{\mathbf{x}}}^{des}\right]$ representing the desired state vector. Despite its simplicity, this control action is not robust technique because of the linerization it requires for guaranteeing the stability. Hence, this aspect constitutes another way to stress the necessity of introducing a robust technique.

Remark 3.1. *Note that* $\mathbf{u}^*$ *depends on both* $f(\tilde{\mathbf{x}})$ *and* $\Delta f(\tilde{\mathbf{x}})$. *This will be useful in what follows to understand the condition of insensitivity of the proposed methodology to them.*

3.1.1 Control Architecture

Generally, when dealing with adaptive control, the control input is split in two terms [18, 19]

$$\mathbf{u} = \mathbf{u}_{PID} + \mathbf{u}_s, \tag{13}$$

where $\mathbf{u}_{PID}$ covers the role of the so-called equivalent control $\mathbf{u}_{eq}$ whereas $\mathbf{u}_s$ is the supervisory control. This latter is an additional control that keeps the system state within some defined boundaries and guarantees

the stability of the dynamical system while the $\mathbf{u}_{PID}$ exploits a gradient-based adaptation law for updating its gains providing robustness of the control. The design of both $\mathbf{u}_s$ and $\mathbf{u}_{PID}$ that is intended to be used here has been defined in [14] and therefore only the key concepts are reported in the followings.

3.1.2 Design of the Supervisory Control

The primary role of the supervisory control $\mathbf{u}_s$ is to keep the system state inside a designed constraint set

$$\mathfrak{C} = \{\mathbf{x} \in \mathbb{R}^{2n} | \, ||\mathbf{x}|| \leq M_{\mathbf{x}}\}, \tag{14}$$

where $M_{\mathbf{x}}$ is a pre-specified parameter usually chosen such that $M_{\mathbf{x}} \geq \ ||\mathbf{y}||_{\infty}$. Its design relies on the errors dynamics and the Lyapunov criterion to guarantee the stability of the system. Hence, to asymptotically attain the zero-error condition, the following Lyapunov function candidate is considered

$$V_e = \frac{1}{2}\mathbf{e}^T \mathbf{\Phi} \mathbf{e}. \tag{15}$$

Observe that V_e represents an *output error energy* measuring the distance from a representative point in the state space to the desired output. Therefore, a plausible strategy to reach it is to exercise a control action that strictly decreases V_e. Before continuing this analysis, it is better to recall the role of the matrix $\mathbf{\Phi}$. Generally, it is defined as a positive definite and symmetric matrix that springs out as the solution of the Lyapunov equation [20]

$$\mathbf{A}^T \mathbf{\Phi} + \mathbf{\Phi} \mathbf{A} = -\mathbf{Q}, \tag{16}$$

where matrix $\mathbf{Q} \in \mathbb{R}^{2n \times 2n}$ is a given, positive definite symmetric matrix whereas matrix $\mathbf{A} \in \mathbb{R}^{2n \times 2n}$ pops out by rewriting the error dynamic as

$$\dot{\mathbf{e}} = \mathbf{A}\mathbf{e} + \mathbf{B}(\mathbf{u}^* - \mathbf{u}_{PID} - \mathbf{u}_s) \tag{17}$$

where the structure of both $\mathbf{A}$ and $\mathbf{B}$ is

$$\mathbf{A} = \begin{bmatrix} \mathbf{0} & \mathbf{I} \\ -\mathbf{k}_0 & -\mathbf{k}_1 \end{bmatrix} \quad \text{and} \quad \mathbf{B} = \begin{bmatrix} \mathbf{0} \\ g(\mathbf{x}, \dot{\mathbf{x}}) \end{bmatrix}, \tag{18}$$

note that $\mathbf{k}_0 \in \mathbb{R}^{n \times n}$ and $\mathbf{k}_1 \in \mathbb{R}^{n \times n}$ are diagonal matrices whose coefficients are chosen such that the roots of the characteristic polynomial, associated with the differential equation $\ddot{\tilde{\mathbf{e}}} + \mathbf{k}_1 \dot{\tilde{\mathbf{e}}} + \mathbf{k}_0 \tilde{\mathbf{e}} = \mathbf{0}$, belong to the left-half complex plane. This aspect is fundamental to guarantee the stability of the system and the convergence to zero of the error as time goes to infinity.

Hence, the design of $\mathbf{u}_s$ must comply with the decrease of V_e, which means that it must meet

$$\dot{V}_e < 0. \tag{19}$$

The derivative of the Lyapunov function can be computed as follows

$$\begin{aligned}\dot{V}_e &= \frac{1}{2}(\dot{\mathbf{e}}^T\mathbf{\Phi}\mathbf{e} + \mathbf{e}^T\mathbf{\Phi}\dot{\mathbf{e}}) \\ &= \frac{1}{2}(\mathbf{e}^T(\mathbf{A}^T\mathbf{\Phi} + \mathbf{\Phi}\mathbf{A})\mathbf{e} + 2\mathbf{e}^T\mathbf{\Phi}\mathbf{B}(\mathbf{u}^* - \mathbf{u}_{PID} - \mathbf{u}_s)) \\ &= -\frac{1}{2}\mathbf{e}^T\mathbf{Q}\mathbf{e} + \mathbf{e}^T\mathbf{\Phi}\mathbf{B}(\mathbf{u}^* - \mathbf{u}_{PID} - \mathbf{u}_s) \\ &\leq -\frac{1}{2}\mathbf{e}^T\mathbf{Q}\mathbf{e} + |\mathbf{e}^T\mathbf{\Phi}\mathbf{B}|(|\mathbf{u}^*| + |\mathbf{u}_{PID}|) - \mathbf{e}^T\mathbf{\Phi}\mathbf{B}\mathbf{u}_s.\end{aligned} \tag{20}$$

Therefore, to satisfy, the supervisory controller can be chosen as

$$\mathbf{u}_s = \text{sgn}(\mathbf{e}^T\mathbf{\Phi}\mathbf{B})(|\mathbf{u}^*| + |\mathbf{u}_{PID}|). \tag{21}$$

However, with this design of $\mathbf{u}_s$, it constantly intervenes in the control process. Further, the presence of *sgn* function leads to chattering. Therefore, to adhere with its supervisory definition and to reduce the chattering the set of constraints $\mathfrak{C}$ is used. In particular, the Indicator function I_f is introduced in the $\mathbf{u}_s$ design as follows

$$\tilde{\mathbf{u}}_s = I_f\,\mathbf{u}_s \quad \text{where} \quad I_f = \begin{cases} 1, & V_e > V_M, \\ 0, & V_e \leq V_M, \end{cases} \tag{22}$$

and

$$V_M = \frac{1}{2}\lambda_{min}(\mathbf{\Phi})(M_{\mathbf{x}} - ||\mathbf{y}||_\infty)^2, \tag{23}$$

where $\lambda_{min}(\mathbf{\Phi})$ is the minimum eigenvalue of the Lyapunov matrix $\mathbf{\Phi}$ [14, 20]. The introduction of the Indicator function completes its design. Indeed, thanks to this modification, $\tilde{\mathbf{u}}_s$ would intervene in the control process only when the system's state diverges from the desired over the limits imposed by $M_{\mathbf{x}}$.

Remark 3.2. *Is worth observing that the value of* $\mathbf{u}^*$ *inside Eq.*(21) *is bounded above. Indeed, rearranging Equation* (12) *it becomes possible finding an estimate for* $\mathbf{u}^*$ *of the type* $\mathbf{u}^{*,u} = \mathbf{g}^{-1}\big(\boldsymbol{\delta}^u + f^u + \Delta f^u + |\ddot{\tilde{\mathbf{x}}}^{des}| + |\mathbf{k}_0\tilde{\mathbf{e}}| + |\mathbf{k}_1\dot{\tilde{\mathbf{e}}}|\big)$.

3.1.3 PID Adaptive Laws

The main control activity is then delegated to an Adaptive PID (APID) which adjusts its control action by automatically tuning its gains. The adaptation laws are derived with the aim to reach the so-called sliding mode $\mathcal{S} = 0$ (i.e. insensitivity to external disturbances) where $\mathcal{S}$ is the so-called sliding surface defined as [19]

$$\mathcal{S} = \dot{\tilde{\mathbf{x}}} - \mathbf{x}_r, \tag{24}$$

where the reference signal $\mathbf{x}_r$ is

$$\mathbf{x}_r = \dot{\tilde{\mathbf{x}}}^{des} + \mathbf{k}_1\tilde{\mathbf{e}} + \mathbf{k}_0 \int \tilde{\mathbf{e}}\, dt. \tag{25}$$

Remark 3.3. *When the sliding mode occurs one has*

$$\mathcal{S} = 0 \quad \textit{and} \quad \dot{\tilde{\mathbf{x}}} = \mathbf{x}_r, \tag{26}$$

this, substituted in the derivative of $\mathbf{x}_r$, $\dot{\mathbf{x}}_r = \ddot{\tilde{\mathbf{x}}}^{des} + \mathbf{k}_1\dot{\tilde{\mathbf{e}}} + \mathbf{k}_0\tilde{\mathbf{e}}$, *returns* $\ddot{\tilde{\mathbf{e}}} + \mathbf{k}_1\dot{\tilde{\mathbf{e}}} + \mathbf{k}_0\tilde{\mathbf{e}} = \mathbf{0}$ *thus revealing that, when the system is in the sliding mode, it becomes insensitive to external disturbances. On the other hand, when* $\mathcal{S} \neq \mathbf{0}$, $\ddot{\tilde{\mathbf{e}}} + \mathbf{k}_1\dot{\tilde{\mathbf{e}}} + \mathbf{k}_0\tilde{\mathbf{e}} = g(\mathbf{x}, \dot{\mathbf{x}})(\mathbf{u}^* - \mathbf{u}_{PID} - \mathbf{u}_s)$ *and therefore the system is not fully insensitive to external disturbances since they appears inside* $\mathbf{u}^*$.

To guarantee approaching the sliding mode the Lyapunov function approach is exploited and the Lyapunov function candidate is then chosen as

$$V = \frac{1}{2}\mathcal{S}^2. \tag{27}$$

Hence requiring that $\mathcal{S}(t) \to \mathbf{0}$ for $t \to \infty$ coincide with reducing V. Consequently, the gradient method is applied to choose the gains which take directions of maximum slope over V. Now, a common expression for a PID controller that can compensate for the gravity acceleration is

$$\mathbf{u}_{PID} = \mathbf{K}_P\tilde{\mathbf{e}} + \mathbf{K}_I \int \tilde{\mathbf{e}}\, dt + \mathbf{K}_D\dot{\tilde{\mathbf{e}}} \; + g\mathbf{e}_3, \tag{28}$$

using the gradient method and the chain rule, it is possible to obtain the adaptation laws for the control gain matrices $\mathbf{K}_P$, $\mathbf{K}_I$ and $\mathbf{K}_D$

$$\dot{\mathbf{K}}_{P,ii} = -\gamma\frac{\partial \mathcal{S}\dot{\mathcal{S}}}{\partial \mathbf{K}_P} = -\gamma\frac{\partial \mathcal{S}\dot{\mathcal{S}}}{\partial \mathbf{u}_{PID}}\frac{\partial \mathbf{u}_{PID}}{\partial \mathbf{K}_P} = -\gamma\mathcal{S}\tilde{\mathbf{e}}\ , \tag{29a}$$

$$\dot{\mathbf{K}}_{I,ii} = -\gamma\frac{\partial \mathcal{S}\dot{\mathcal{S}}}{\partial \mathbf{K}_I} = -\gamma\frac{\partial \mathcal{S}\dot{\mathcal{S}}}{\partial \mathbf{u}_{PID}}\frac{\partial \mathbf{u}_{PID}}{\partial \mathbf{K}_I} = -\gamma\mathcal{S}\int \tilde{\mathbf{e}}\, dt, \tag{29b}$$

$$\dot{\mathbf{K}}_{D,ii} = -\gamma\frac{\partial \mathcal{S}\dot{\mathcal{S}}}{\partial \mathbf{K}_D} = -\gamma\frac{\partial \mathcal{S}\dot{\mathcal{S}}}{\partial \mathbf{u}_{PID}}\frac{\partial \mathbf{u}_{PID}}{\partial \mathbf{K}_D} = -\gamma\mathcal{S}\dot{\tilde{\mathbf{e}}}\ , \tag{29c}$$

where minus is placed opposite to the energy flow V and $\gamma \in \mathbb{R}^+$ is called learning rate[1].

To conclude, the behaviour of the controller can be resumed as follows: if $\mathbf{u}_s = \mathbf{0}$, the PID gains adapt themselves to decrease V to zero (i.e. reach the sliding mode) whereas if $\mathbf{u}_s \neq \mathbf{0}$, the PID gains are not able to decrease V and then also V_e under V_M.

[1]To avoid cumbersome notation the subscripts ii (emphasizing the diagonal structure of the gain matrices) has been inserted only to the left hand side of the equation intending the derivative operation to be carried out component-wise. As typical in the literature [21].

3.2 Design of the Parallel Components

The parallel component is chosen to track the desired trajectory of the load, in other words it is necessary to define $\mathbf{v}_i^{\parallel}$ s.t. $\mathbf{x}_L \longrightarrow \mathbf{x}_L^{des}$ while $t \longrightarrow \infty$.

Let's consider the load Equation (4). Since the translational dynamic is influenced only by the terms parallel to $\mathbf{q}_i$ then, it is possible to derive $\mathbf{v}_i^{\parallel}$ as

$$\mathbf{v}_i^{\parallel} = m_i l_i ||\boldsymbol{\omega}_i||^2 \mathbf{q}_i + t_i \mathbf{q}_i + \frac{m_i}{m_L} \mathbf{q}_i \mathbf{q}_i^T \sum_{j=1}^{n} t_j \mathbf{q}_j - (\mathbf{q}_i \cdot \mathbf{f}_{i,w}) \mathbf{q}_i, \tag{30}$$

where t_i represent the tension along the i^{th} link. To find the tensions to be applied along the links, it is enough to substitute (30) into (4) and make some arrangements to see that

$$(\ddot{\mathbf{x}}_L + g\mathbf{e}_3) = \frac{1}{m_L} \sum_{j=1}^{n} t_j \mathbf{q}_j + \Big(\sum_{i=1}^{n} m_i \mathbf{q}_i \mathbf{q}_i^T + m_L \mathbf{I} \Big)^{-1} \mathbf{f}_{L,w}, \tag{31}$$

and considering $\Big(\sum_{i=1}^{n} \frac{m_i}{m_L} \mathbf{q}_i \mathbf{q}_i^T + \mathbf{I} \Big)^{-1}$ as a dimensionless distribution mass-matrix $\mathbf{M}$, one has

$$(\ddot{\mathbf{x}}_L + g\mathbf{e}_3) = \frac{1}{m_L} \sum_{j=1}^{n} t_j \mathbf{q}_j + \frac{1}{m_L} \mathbf{M}\, \mathbf{f}_{L,w}, \tag{32}$$

which leads to

$$\ddot{\mathbf{x}}_L = -g\mathbf{e}_3 + \frac{1}{m_L} \mathbf{w} + \frac{1}{m_L} \boldsymbol{\delta}(t), \tag{33}$$

where $\boldsymbol{\delta}(t)$ represents the effect of the external disturbance whereas $\mathbf{w}$ is the wrench that act on the load. Rearranging this equation in the form of Newton' law, one has

$$\mathbf{w} = m_L \big((\ddot{\mathbf{x}}_L + g\mathbf{e}_3) - \frac{1}{m_L} \boldsymbol{\delta}(t) \big), \tag{34}$$

grouping the terms at RHS inside $\mathbf{u}$, returns

$$\mathbf{w}^{des} = m_L \mathbf{u}, \tag{35}$$

where the superscript des in $\mathbf{w}^{des}$ emphasizes that the control action coincides, up to the m_L constant, with the wrench that should be generated on the load to track the desired trajectory. In other words, it represents the action necessary to compensate for the external forces, disturbances and then correct the tracking error. As a consequence, the tensions necessary to steer the load, for $n \geq 3$, can be found as

$$\mathbf{t} = \mathbf{W}^{\dagger} \mathbf{w}^{des} + \mathbf{N}\boldsymbol{\lambda}, \tag{36}$$

where $\mathbf{W} = [\mathbf{q}_1, \mathbf{q}_2, ..., \mathbf{q}_n] \in \mathbb{R}^{3 \times n}$ is the so-called wrench matrix, $\mathbf{W}^{\dagger} = \mathbf{W}^T (\mathbf{W}\mathbf{W}^T)^{-1}$ is its pseudo-inverse, $\mathbf{N} \in \mathbb{R}^{(n-3) \times n}$ contains the vector that span the kernel of $\mathbf{W}$ and $\boldsymbol{\lambda} \in \mathbb{R}^{(n-3)}$.

3.3 Design of the Orthogonal Components

The normal component is chosen to reach the desired *relative* configuration of the system, in other words it becomes necessary to define $\mathbf{v}_i^{\perp}$ s.t. $\mathbf{q}_i \longrightarrow \mathbf{q}_i^{des}$ while $t \longrightarrow \infty$. This correspond to the tracking problem on $\mathbb{S}^2$ which was studied in [2, 22]. In particular, the direction and angular velocity errors, are defined as follows

$$\mathbf{e}_{\mathbf{q}_i} = \mathbf{q}_i^{des} \times \mathbf{q}_i \quad \text{and} \quad \mathbf{e}_{\boldsymbol{\omega}_i} = \boldsymbol{\omega}_i + \hat{\mathbf{q}}_i^2 \boldsymbol{\omega}_i^{des}, \tag{37}$$

whereas, the angular acceleration is

$$\dot{\boldsymbol{\omega}}_i = -K_{\mathbf{q}_i}\mathbf{e}_{\mathbf{q}_i} - K_{\boldsymbol{\omega}_i}\mathbf{e}_{\boldsymbol{\omega}_i} - (\mathbf{q}_i \cdot \boldsymbol{\omega}_i^{des})\dot{\mathbf{q}}_i - \hat{\mathbf{q}}_i^2 \dot{\boldsymbol{\omega}}_i^{des}, \tag{38}$$

for positive gains $K_{\mathbf{q}_i}$ and $K_{\boldsymbol{\omega}_i}$. Now, substituting (31) into (6) yields to

$$\dot{\boldsymbol{\omega}}_i = \frac{1}{m_L l_i}\hat{\mathbf{q}}_i \sum_{j=1}^{n} t_j \mathbf{q}_j - \frac{1}{m_i l_i}\hat{\mathbf{q}}_i \mathbf{v}_i^{\perp} - \frac{1}{m_i l_i}\hat{\mathbf{q}}_i \mathbf{f}_{i,w}, \tag{39}$$

and $\mathbf{v}_i^{\perp} = -\hat{\mathbf{q}}_i^2 \mathbf{v}_i$ leads us to the expression for the normal component $\mathbf{v}_i^{\perp}$ [4]

$$\mathbf{v}_i^{\perp} = m_L l_i \hat{\mathbf{q}}_i(-K_{\mathbf{q}_i}\mathbf{e}_{\mathbf{q}_i} - K_{\boldsymbol{\omega}_i}\mathbf{e}_{\boldsymbol{\omega}_i} - (\mathbf{q}_i \cdot \boldsymbol{\omega}_i^{des})\dot{\mathbf{q}}_i - \hat{\mathbf{q}}_i^2 \dot{\boldsymbol{\omega}}_i^{des}) - \frac{m_i}{m_L}\hat{\mathbf{q}}_i^2 \sum_{j=1, j\neq i}^{n} t_j \mathbf{q}_j + \hat{\mathbf{q}}_i^2 \mathbf{f}_{i,w}. \tag{40}$$

3.4 Quadrotor's Attitude Control

To fully control the overall system, the attitude control of each quadrotor must be included. Hence, as done in [23], the control moment for each quadrotor is

$$\mathbf{m}_i = -K_{\mathbf{R}_i}\mathbf{e}_{\mathbf{R}_i} - K_{\boldsymbol{\Omega}_i}\mathbf{e}_{\boldsymbol{\Omega}_i} + \boldsymbol{\Omega}_i \times \mathbf{J}_i\boldsymbol{\Omega}_i - \mathbf{J}_i(\hat{\boldsymbol{\Omega}}_i \mathbf{R}_i^T \mathbf{R}_i^c \boldsymbol{\Omega}_i^c - \mathbf{R}_i^T \mathbf{R}_i^c \dot{\boldsymbol{\Omega}}_i^c), \tag{41}$$

where $\cdot^c$ stands for *controlled variables*, $\cdot^{\vee}$ denotes the *vee map*:$\cdot^{\vee} : \mathfrak{so}(3) \to \mathbb{R}^3$, $K_{\mathbf{R}_i}$, $K_{\boldsymbol{\Omega}_i}$ are diagonal positive-gain matrices and $\mathbf{e}_{\mathbf{R}_i}$, $\mathbf{e}_{\boldsymbol{\Omega}_i}$ are the errors for the attitude dynamics defined as

$$\mathbf{e}_{\mathbf{R}_i} = \frac{1}{2}(\mathbf{R}_i^{Tc}\mathbf{R}_i - \mathbf{R}_i^T \mathbf{R}_i^c)^{\vee} \quad \text{and} \quad \mathbf{e}_{\boldsymbol{\Omega}_i} = \boldsymbol{\Omega}_i - \mathbf{R}_i^T \mathbf{R}_i^c \boldsymbol{\Omega}_i^c, \tag{42}$$

Equation (41) together with

$$f_i = \mathbf{v}_i \cdot \mathbf{R}_i \mathbf{e}_3, \tag{43}$$

constitute the control actions for each agent of the system. The overall control scheme is depicted in Figure 3.

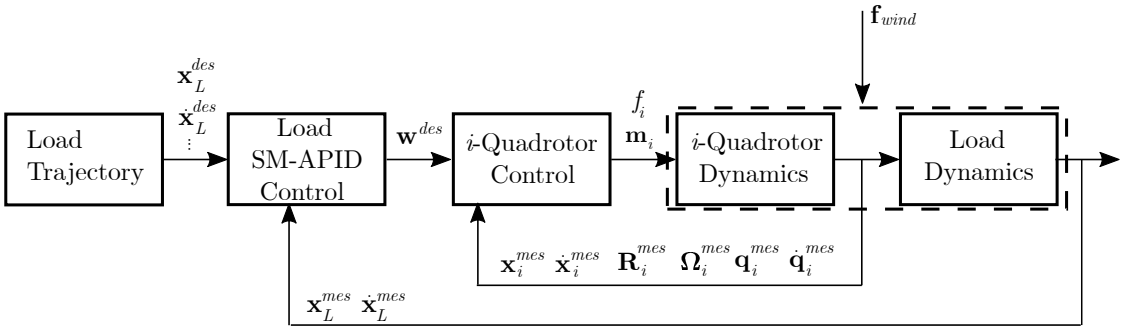

Fig. 3: Control scheme: it illustrates the various blocks that define the control logic and the quantities that are exchanged while the system is working.

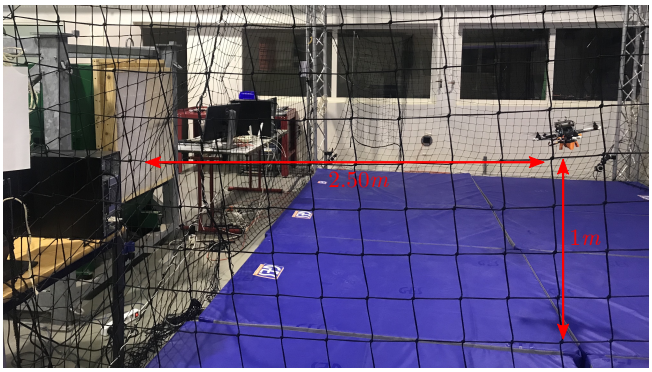

(a) Wind force estimation: quadrotor windswept during the experimental estimation of the aerodynamic force.

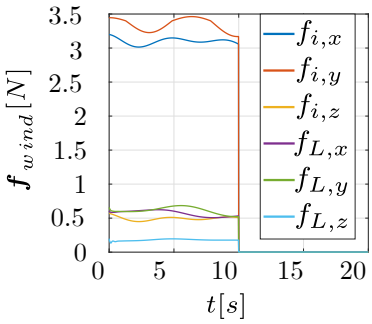

(b) Wind forces: wind force components acting on the aerial system.

Fig. 4: Wind force estimation and profiles.

4 SIMULATIONS

To shed some light on the peculiarities of the proposed approach numerical simulations are made. In particular, the tracking performances of different control are compared. An aerial system, with three rigid links and three quadrotors transporting a point-mass load, is considered. The task to be completed involves guiding the load along an elliptical trajectory. Both the load and the quadrotors were subjected to a wind that persisted for the entire simulation. To compute the aerodynamic forces $\mathbf{f}_{L,w}$ and $\mathbf{f}_{i,w}$ empirical equations are used for the former and some experimental measures for the latter, respectively. In particular, $\mathbf{f}_{L,w} = \frac{1}{2}C_d A_L \rho (v_w - ||\dot{\mathbf{x}}_L(t)||)^2 \mathbf{e}_\infty$ where $\mathbf{e}_\infty$ represent the direction of the relative velocity (i.e. unit vector) and whose parameters were reported in the Table 1 together with other useful parameters for the simulation. The value of $\mathbf{f}_{i,w}$ is difficult to derive empirically since the shape of quadrotors is complex and not unified. Consequently, its value was estimated through experimental tests carried out at the LS2N arena [24]. In particular, thanks to the use of a fan (shown in Figure 4a) and a first-order observer on a quadrotor, it was possible to determine a link between wind force and wind speed. This, together with the Dryden's model, allowed us to derive the wind forces acting on the drones as shown in Figure 4b. All this continues to be an approximation of reality but their proper modelling is beyond the scope of this paper. What is of interest instead, is to show that the presence of a persistent and time-varying force of aerodynamic nature, can be managed by the proposed control.

Table 1: Simulation parameters.

Parameter	Value	Parameter	Value
A_x	$0.8\,m$	$m_1 = m_2 = m_3$	$1.15\,kg$
A_y	$0.5\,m$	$l_1 = l_2 = l_3$	$1\,m$
m_L	$0.5\,kg$	$\mathbf{k}_0$	$\text{diag}\begin{pmatrix}0.1 & 0.1 & 0.1\end{pmatrix}$
D	$0.2\,m$	$\mathbf{k}_1$	$\text{diag}\begin{pmatrix}1 & 1 & 1\end{pmatrix}$
C_d	0.5	$\mathbf{J}_1 = \mathbf{J}_2 = \mathbf{J}_3$	$\text{diag}\begin{pmatrix}0.01 & 0.1 & 0.14\end{pmatrix} kg \cdot m^2$
ρ	$1.2\ \frac{kg}{m^3}$	$\mathbf{K}_P(0) = \mathbf{K}_I(0) = \mathbf{K}_D(0)$	$\text{diag}\begin{pmatrix}5 & 5 & 5\end{pmatrix}$
A_L	$\frac{\pi D^2}{4}$	$\mathbf{K}_P = \mathbf{K}_I = \mathbf{K}_D$	$\text{diag}\begin{pmatrix}5 & 5 & 5\end{pmatrix}$
γ	10	$K_{\mathbf{q}_i} = K_{\boldsymbol{\omega}_i} = K_{\mathbf{R}_i} = K_{\boldsymbol{\Omega}_i}$	$\text{diag}\begin{pmatrix}5 & 5 & 5\end{pmatrix}$
T	$20s$	$\boldsymbol{\Omega}_i(0) = \dot{\mathbf{x}}_L(0) = \boldsymbol{\omega}_i(0) = \boldsymbol{\omega}_i^{des}$	$\begin{bmatrix}0 & 0 & 0\end{bmatrix}$
$\mathbf{R}_i(0)$	$\mathbf{I}$	$\mathbf{x}_L^{des}$	$\begin{bmatrix}A_x\cos(\omega t) & A_y\sin(\omega t) & 0\end{bmatrix} m$
$\mathbf{i}_i^{des}$	$\mathbf{e}_1$	$\mathbf{x}_L(0)$	$\begin{bmatrix}A_x & 0 & 0.5\end{bmatrix} m$
$\mathbf{q}_1(0)$	$\begin{bmatrix}\sin 80° & 0 & -\cos 80°\end{bmatrix}$	$\mathbf{q}_1^{des}$	$\begin{bmatrix}0 & -\sin 40° & -\cos 40°\end{bmatrix}$
$\mathbf{q}_2(0)$	$\begin{bmatrix}0 & \sin 80° & -\cos 80°\end{bmatrix}$	$\mathbf{q}_2^{des}$	$\begin{bmatrix}\sin 40° & 0 & -\cos 40°\end{bmatrix}$
$\mathbf{q}_3(0)$	$\begin{bmatrix}-\sin 80° & 0 & -\cos 80°\end{bmatrix}$	$\mathbf{q}_3^{des}$	$\begin{bmatrix}0 & \sin 40° & -\cos 40°\end{bmatrix}$

The initial configuration of the system and some phases of the task are shown in the following figure with the purpose of showing the overall behaviour of the system during the execution of the task Figure 5. It is noteworthy that the system properly reconfigures itself to reach the desired output while counteracting the external disturbances. In addition, the sliding variables trends and the gains curves were reported in Figures 7 and 6, respectively. Figure 6 shows that k_P and k_I gains stabilize after a transitory phase that last, approximately, 5 seconds whereas k_D gains continue to adjust in order to reach the sliding surface. Indeed, from Figure 7, one can see that the sliding variable values first decrease and then oscillate about zero for the entire duration of the simulation. The attainment of the sliding condition in finite time is not guaranteed with this design. Indeed, in Section 3.1.3, the main requirement states as $\mathcal{S} \to 0$ for $t \to \infty$. It should also be noted that, since this condition is not reached in the first 10 seconds, when the wind changes intensity, Figure 4b, the sliding variables locally increase their value and then decrease again. Thus, although the system may never achieve effective insensitivity from external disturbances, it does reduce their effect on the system by making the controller more robust. This can be observed with the following comparison.

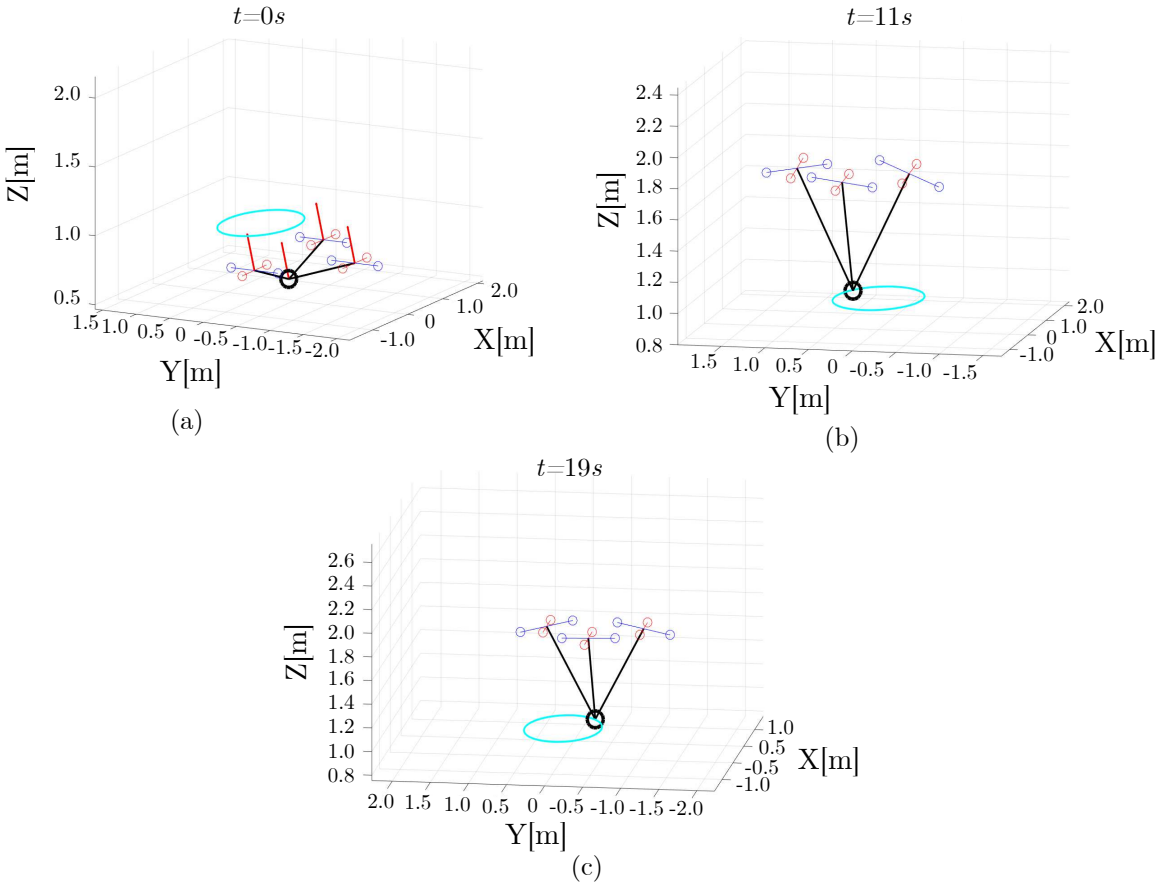

Fig. 5: Simulation phases: snapshots of the system during the simulation with SM-APID control. The snapshots show the system in (a) the initial condition $t = 0s$, (b) after one turn along the ellipses were the wind suddenly disappears $t = 11s$ and (c) in the final phase of the task $t = 19s$. The red arrows, where present, show the presence and direction of the aerodynamic force acting on the quadrotor and load.

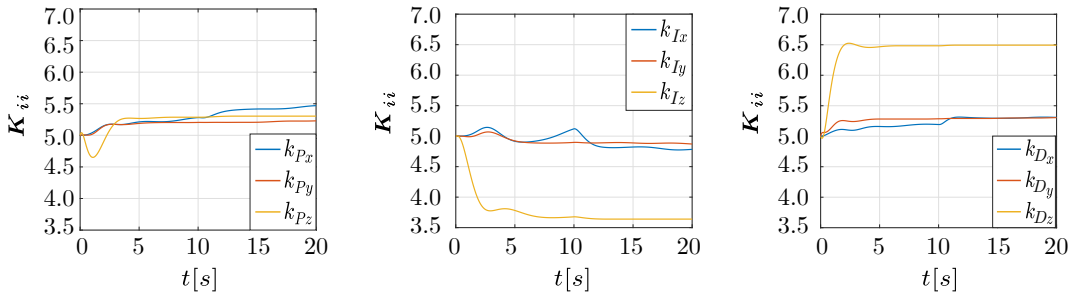

Fig. 6: Control gains: trends of the tuned gains in time.

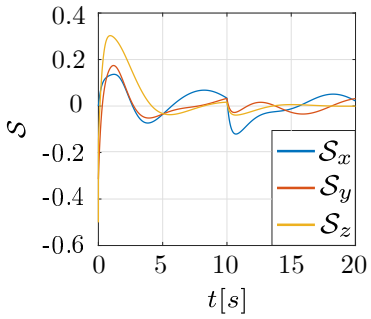

Fig. 7: Sliding variables: trends of the sliding variables in time.

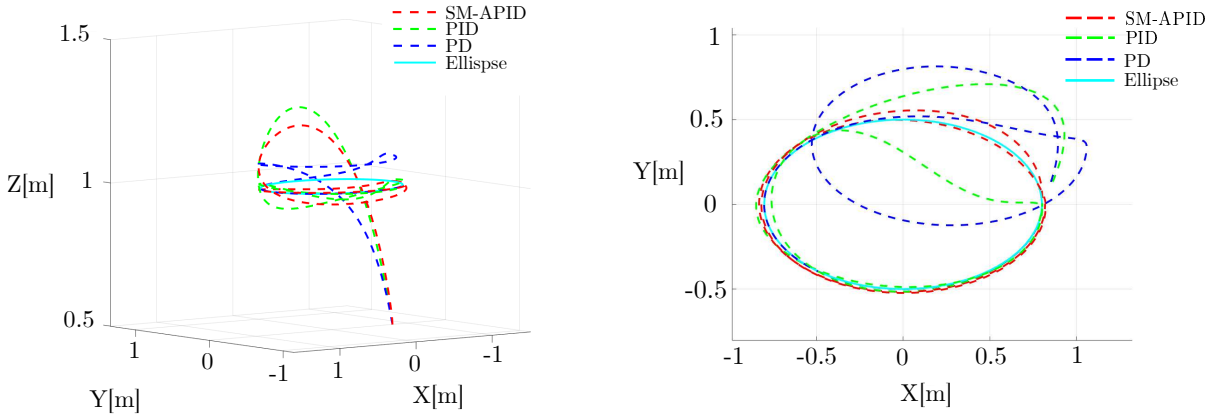

Fig. 8: Trajectories comparison: spatial and planar view of the undertaken load trajectory.

Comparisons are made by examining the controller developed in [4] (a PD control) and a revised version of it [10] (PID). To qualitatively compare their performance, reference can be made to Figures 8 and 9. The first two images show the trajectory followed by the load during the simulation with different control techniques. The third image shows the error trends along with the three directions (x, y and z). Therefore, from these pictures, it can be inferred that both PD and PID controllers fail to accomplish the task. In fact, the PD only manages to keep the error within a certain value. Instead the PID, thanks to the integral part, seems to recover the trajectory. However, during the recovery phase, the quadrotors perform a sudden manoeuvre which could not be achievable in reality since it could lead the system to crash. Indeed, the gains of these controllers (PD and PID) are chosen sufficiently high in order to guarantee the performance shown here and then to make comparisons. In general, with lower gain values both the controllers are not able to conclude the task. On the other hand, this result confirms the robustness of the proposed controller.

Additional Figures 10 and 11 also show the error trend of the attitude of each quadrotor and the error of the configuration (link directions) as well. It should be noted that the attitude and configuration errors are quite similar for both the PD and PID. In contrast, in the case of the SM-APID, it can be seen that the $e_{\mathbf{R}}$

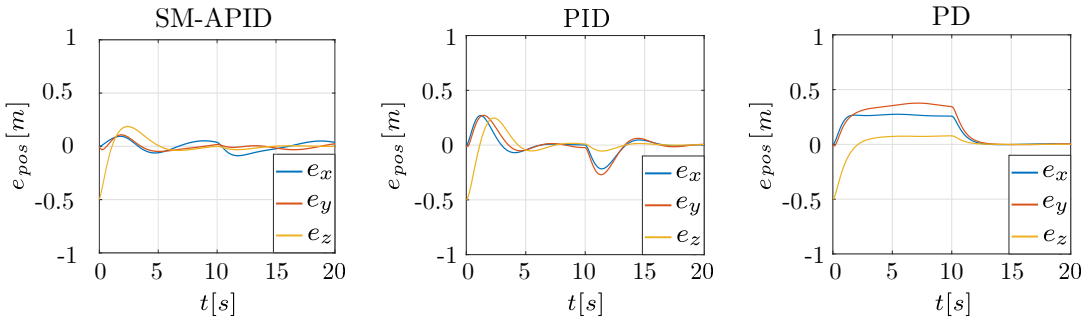

Fig. 9: Position errors: the components of the position errors for the three study cases are hereby depicted.

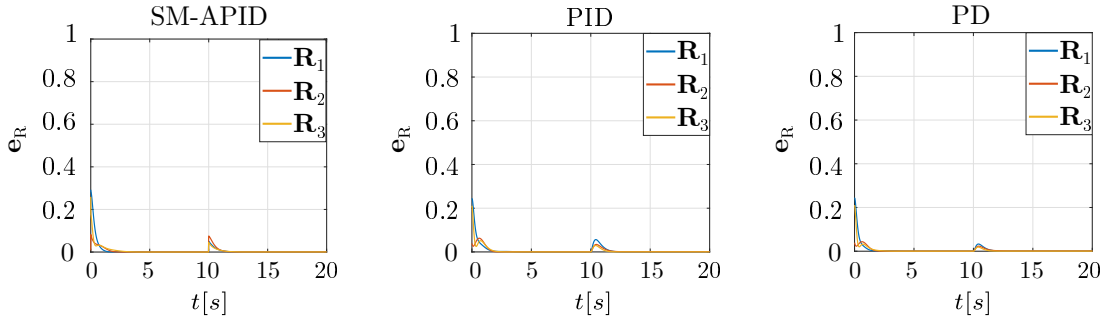

Fig. 10: Attitude errors: orientation error for each quadrotors in the three study cases is given. The error equation on $SO(3)$ is: $e_{\mathbf{R}} = \frac{1}{2}\,\mathrm{trace}(\mathbf{I} - \mathbf{R}_i^{Tc}\mathbf{R}_i)$.

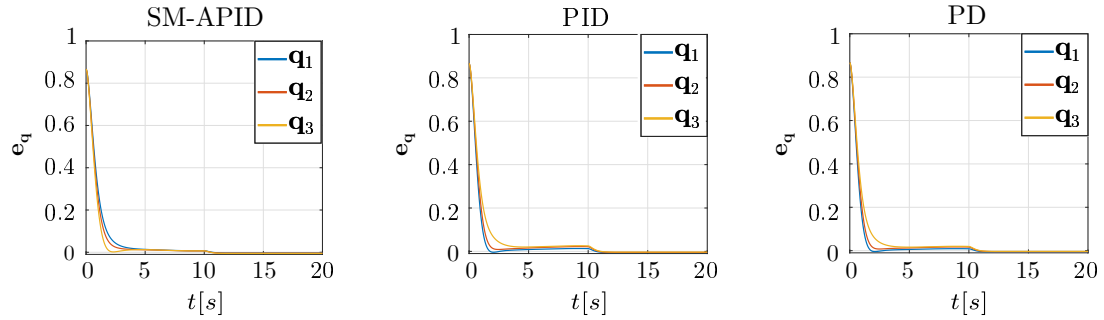

Fig. 11: Configuration errors: the link direction error for each bar in the three study cases is reported. The error equation on $\mathbb{S}^2$ is: $e_{\mathbf{q}} = 1 - \mathbf{q}_i \cdot \mathbf{q}_i^{des}$.

converges slightly faster at zero while $e_{\mathbf{q}}$ error remains lower than PD and PID controllers. However, in all cases $e_{\mathbf{q}}$ is not zero because the controller does not compensate for the external disturbances. The reason why it is lower for the proposed controller is due to the presence of the term $\hat{\mathbf{q}}_i^2\mathbf{f}_{i,w}$ in Equation (40). This is absent in the other two controllers.

On the other hand, a tangible way to compare the performances is provided by Table 2. It makes a statistical analysis of the errors. In this case, Table 2 refers to the position error only since, in this example, a tracking task is considered. To conclude, Table 2 qualitatively confirms that, in general, the errors (MEAN, STD or RMSE) along each direction are smaller in the case of the SM-APID controller.

Table 2: Error analysis: the Mean, STD and RMSE values for the trajectory tracking problems is computed for the three study cases.

Trajectory	Control Type	Statistics	Load position (m)		
			x	y	z
Ellipses	PD	MEAN	0.137	0.173	0.008
		STD	0.124	0.163	0.094
		RMSE	0.185	0.238	0.094
Ellipses	PID	MEAN	$1e^{-4}$	$2e^{-4}$	$1e^{-4}$
		STD	0.093	0.107	0.103
		RMSE	0.093	0.107	0.103
Ellipses	SM-APID	MEAN	0.002	0.001	$3e^{-4}$
		STD	0.049	0.034	0.090
		RMSE	0.049	0.034	0.090

5 CONCLUSION

The analogy between chaotic systems and wind considered as such enabled to make current controllers more robust in presence of external disturbances. In particular, the design of a controller to guide an aerial system subjected to wind gusts was tackled. Both an online tuning gains PID and a supervisory control were integrated with existing techniques to steer the system immersed in a wind field. Furthermore, simulations showed the validity of our approach thus confirming the validity of this analogy.

Despite the presence of many existing techniques for the estimation and compensation of aerodynamic forces, this is the first time that a controller of this type has been used in this context. Futures effort aims to develop a model that takes into account the flexibility of the cables and in doing experimental validation of our approach.

REFERENCES

[1] Tognon, M., and Franchi, A., 2020, *Theory and Applications for Control of Aerial Robots in Physical Interaction Through Tethers* Springer Tracts in Advanced Robotics.

[2] Bullo, F., and Lewis, A. D., 2005, *Geometric control of mechanical systems: modeling, analysis, and design for simple mechanical control systems* Springer, Texts in Applied Mathematics.

[3] Jean, L., 2009, *Analysis and control of nonlinear systems: A flatness-based approach* Springer Science & Business Media.

[4] Lee, T., Sreenath, K., and Kumar, V., 2013, "Geometric control of cooperating multiple quadrotor uavs with a suspended payload," *52nd IEEE Conference on Decision and Control*.

[5] Koushil, S., Taeyoung, L., and Vijay, K., 2013, "Geometric control and differential flatness of a quadrotor uav with a cable-suspended load," *52nd IEEE Conference on Decision and Control*.

[6] Wu, G., and Sreenath, K., 2014, "Geometric control of multiple quadrotors transporting a rigid-body load," *53rd IEEE Conference on Decision and Control*.

[7] Lee, T., 2014, "Geometric control of quadrotor uavs transporting a cable-suspended rigid body," *IEEE Transactions on Control Systems Technology*.

[8] A., G. F., and Taeyoung, L., 2016, "Stabilization of a rigid body payload with multiple cooperative quadrotors," *Journal of Dynamic Systems, Measurement, and Control*.

[9] Kotaru, P., Wu, G., and Sreenath, K., 2018, "Differential-flatness and control of quadrotor(s) with a payload suspended through flexible cable(s)," *2018 Indian Control Conference (ICC)*.

[10] Li, G., Ge, R., and Loianno, G., 2021, "Cooperative transportation of cable suspended payloads with mavs using monocular vision and inertial sensing," *IEEE Robotics and Automation Letters*.

[11] Di Paola, V., Ida', E., Zoppi, M., and Caro, S., 2022, "A preliminary study of factors influencing the stiffness of aerial cable towed systems," *ROMANSY, Springer International Publishing*.

[12] Cole, K., and Wickenheiser, A., 2019, "Spatio-temporal wind modeling for uav simulations," *arXiv*.

[13] Yan, J.-J., 2004, "Design of robust controllers for uncertain chaotic systems with nonlinear inputs," *Chaos, Solitons & Fractals*.

[14] Chang, W.-D., and Yan, J.-J., 2005, "Adaptive robust pid controller design based on a sliding mode for uncertain chaotic systems," *Chaos, Solitons & Fractals*.

[15] Waslander, S., and Wang, C., 2009, "Wind disturbance estimation and rejection for quadrotor position control," *AIAA Infotech@Aerospace Conference*.

[16] Sreenath, K., and Kumar, V., 2013, "Dynamics, control and planning for cooperative manipulation of payloads suspended by cables from multiple quadrotor robots," *Robotics: Science and Systems IX*.

[17] Tang, S., Sreenath, K., and Kumar, V., 2014, "Aggressive maneuvering of a quadrotor with a cable-suspended payload," *Robotics: Science and Systems, Workshop on Women in Robotics*.

[18] Hsueh, Y.-C., and Su, S.-F., 2007, "Supervisory controller design based on lyapunov stable theory," *2007 IEEE International Conference on Systems, Man and Cybernetics*.

[19] Yuri, S., Christopher, E., Leonid, F., and Arie, L., 2014, *Sliding Mode Control and Observation* Birkhäuser, New York, NY.

[20] Zabczyk, J., 2020, *Mathematical Control Theory, An Introduction* Birkhäuser, Cham.

[21] Noordin, A., Mohd Basri, M. A., Mohamed, Z., and Mat Lazim, I., 2021, "Adaptive pid controller using sliding mode control approaches for quadrotor uav attitude and position stabilization," *Arabian Journal for Science and Engineering*.

[22] Wu, G., and Sreenath, K., 2015, "Variation-based linearization of nonlinear systems evolving on $so(3)$ and $\mathbb{S}^2$," *IEEE Access*.

[23] Lee, T., Leok, M., and McClamroch, N., 2010, "Geometric tracking control of a quadrotor uav on se(3)," *Proceedings of the IEEE Conference on Decision and Control*.

[24] Erskine, J., Chriette, A., and Caro, S., 2019, "Wrench analysis of cable-suspended parallel robots actuated by quadrotor unmanned aerial vehicles," *Journal of Mechanisms and Robotics*.